Postsynthetic Metal and Ligand Exchange in MFU-4*l*: A Screening Approach toward Functional Metal–Organic Frameworks Comprising Single-Site Active Centers

Dmytro Denysenko,[a] Jelena Jelic,[b] Karsten Reuter,[b] and Dirk Volkmer*[a]

Abstract: The isomorphous partial substitution of Zn^{2+} ions in the secondary building unit (SBU) of MFU-4*l* leads to frameworks with the general formula $[M_xZn_{(5-x)}Cl_4(BTDD)_3]$, in which $x \approx 2$, M = Mn^{II}, Fe^{II}, Co^{II}, Ni^{II}, or Cu^{II}, and BTDD = bis(1,2,3-triazolato-[4,5-b],[4′,5′-i])dibenzo-[1,4]-dioxin. Subsequent exchange of chloride ligands by nitrite, nitrate, triflate, azide, isocyanate, formate, acetate, or fluoride leads to a variety of MFU-4*l* derivatives, which have been characterized by using XRPD, EDX, IR, UV/Vis-NIR, TGA, and gas sorption measurements. Several MFU-4*l* derivatives show high catalytic activity in a liquid-phase oxidation of ethylbenzene to acetophenone with air under mild conditions, among which Co- and Cu derivatives with chloride side-ligands are the most active catalysts. Upon thermal treatment, several side-ligands can be transformed selectively into reactive intermediates without destroying the framework. Thus, at 300 °C, Co^{II}-azide units in the SBU of Co-MFU-4*l* are converted into Co^{II}-isocyanate under continuous CO gas flow, involving the formation of a nitrene intermediate. The reaction of Cu^{II}-fluoride units with H_2 at 240 °C leads to Cu^{I} and proceeds through the heterolytic cleavage of the H_2 molecule.

Introduction

Metal–organic frameworks (MOFs) are coordination polymers featuring an open framework containing potential voids. MOFs represent an exponentially growing research field[1] and have been tested for many different applications such as capture of gases and vapors,[2] gas separation and storage,[3] catalysis,[4] sensing,[5] as luminescent[6] or ferroelectric[7] materials, and as materials for non-linear optics[8] or biomedicine.[9] For each kind of application, the framework properties have to be adjusted according to the specific requirements. However, it is often difficult to synthesize a MOF with desired properties directly. For this reason, post-synthetic modification has been developed as a powerful approach towards functional metal–organic frameworks. The most frequently practiced way for post-synthetic framework modification includes covalent modification(s) of the organic linkers, such as the reaction sequence of nitration or bromination of aromatic moieties, condensation reactions of amines with aldehydes, carboxylic acid derivatives or isocyanates, post-synthetic deprotection and click reactions (cycloaddition to azides).[10] These methods allow the introduction of the desired functional groups into the framework, adjustment of the pore structure, tuning of the breathing properties, and so on. Another common approach towards modified frameworks is represented by the post-synthetic metalation (coordination of metal ions to the functional groups or free coordination sites of organic linkers), which is used for introducing catalytically active or luminescent metal ions into the framework or for improving the sorption properties of the MOF.[11] A post-synthetic linker exchange has been realized for several MOF structures.[12] Finally, post-synthetic metal exchange in secondary building units (SBUs) has been described for different MOF families, whereas in many cases only partial substitution was achieved.[13] We have previously described the post-synthetic exchange of the peripheral (tetrahedrally coordinated) Zn^{II} ions by Co^{II}[14] and Cu^{II}[15] in MFU-4*l*.[16] In addition, the solvent-dependent Zn/Co exchange in MFU-4*l* has been investigated in detail.[17] MFU-4*l*, constructed from deprotonated bis(1*H*-1,2,3-triazolo-[4,5-b],[4′,5′-i])dibenzo-[1,4]-dioxin (BTDD) ligands and $\{Zn_5Cl_4\}^{6+}$ building units, is a large-pore member of the MFU-4 structure family of cubic frameworks featuring exceptionally high thermal and solvolytic stability.[18] A close structural relative to this family, CFA-1, has been shown to undergo Zn/Co exchange under similar reaction conditions.[19] The SBU of these frameworks (and in structurally related molecular Kuratowski-type coordination compounds)[20] includes one octahedrally coordinated (central) metal ion and four tetrahedrally coordinated (peripheral) metal ions. The tetrahedrally coordinated metal ions are structurally related to well-known scorpionate complexes.[21] This coordination principle allows for the stepwise exchange of peripheral metal ions, whereas the central octahedrally coordinated Zn^{2+} ion remains unchanged and the SBU

[a] *D. Denysenko, Prof. Dr. D. Volkmer*
Institute of Physics, Chair of Solid State and Materials Chemistry
University of Augsburg, Universitätsstrasse 1, 86159 Augsburg (Germany)
E-mail: dirk.volkmer@physik.uni-augsburg.de

[b] *Dr. J. Jelic, Prof. Dr. K. Reuter*
Chair of Theoretical Chemistry and Catalysis Research Center
Technische Universität München, Lichtenbergstr. 4
85747 Garching (Germany)

remains intact (Figure 1). This approach allows us to obtain heterometallic derivatives of MFU-4*l*, which were so far unavailable through direct synthesis. We have previously also shown that chloride side-ligands in MFU-4*l* and Cu-MFU-4*l* can be easily substituted by formate ligands.[15] Thermal activation of thus obtained formate MFU-4*l* derivatives led to Zn–H or Cu^{I} species, the latter showing unique chemisorption properties for several simple gas molecules (e.g., H_2, N_2 and O_2).[15] In addition, Co-MFU-4*l* was found to be catalytically active in the heterogeneous oxidation of carbon monoxide.[14] Lastly, MFU-4 and MFU-4*l* frameworks have been studied in technically demanding gas separations such as Xe/Kr[22] or H_2/D_2.[23] Introducing other metal ions into MFU-4*l* structure therefore seems a rewarding research goal in terms of developing functional frameworks. Subsequent ligand exchange allows us to tune the reactivity of metal centers and to perform further transformations including the in situ generation of active metal sites. Additionally, the pore geometry can be optimized for applications such as gas storage and separation. In this manuscript we present the synthesis and characterization of a variety of MFU-4*l* derivatives obtained through post-synthetic metal and ligand exchange leading to a screening approach towards functional metal–organic frameworks comprising open metal sites. Mn-, Fe- and Ni derivatives of MFU-4*l* are presented, which were not considered in our earlier works. The possibilities and limitations of side-ligand exchange reactions are discussed in detail.

Results and Discussion

Post-synthetic modifications of MFU-4*l*

We have previously reported on the complete exchange of peripheral Zn^{2+} ions in MFU-4*l* by Co^{2+} at 140 °C in DMF.[14] Metal exchange with Cu^{2+}, however, can only be conducted at 60 °C (due to the formation of amorphous impurities at higher temperatures) and leads to a partial (≈50 %) substitution.[15] Similarly, other 3d transition-metal ions (Mn^{2+}, Fe^{2+}, and Ni^{2+}) can be introduced into the SBU by dispersing MFU-4*l* crystals into a solution containing a large excess of metal(II) chloride in DMF or DMA at 60 °C. Under these conditions, approximately 40 to 60 % of the peripheral Zn^{2+} ions are substituted leading to frameworks with the general formula $[M_xZn_{(5-x)}Cl_4(BTDD)_3]$, in which $x \approx 2$ and BTDD = bis(1,2,3-triazolato-[4,5-b],[4′,5′-i])dibenzo-[1,4]-dioxin (Scheme 1).

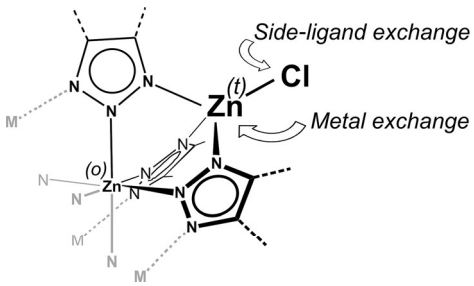

Figure 1. Metal- and side-ligand exchange on the peripheral position in the SBU of MFU-4-type frameworks (a part of the SBU is shown; *t*-tetrahedral, *o*-octahedral; only one out of four tetrahedrally coordinated (= peripheral) Zn centers is shown).

Only in the case of Co^{II} are approximately 3 of 4 Zn^{2+} ions substituted under these conditions, indicating that substitution by Co^{II} is more favorable than that of other 3d transition-metal ions. This is probably due to the highest ligand field stabilization energy (12 D_q^{tet} for tetrahedrally coordinated d^7 metal ions) among the applied metal ions. For Mn^{II}, Fe^{II}, and Cu^{II}, metal exchange at temperatures above 60 °C leads to impure products, as verified by XRPD, IR spectroscopy, and gas sorption measurements. Only in the case of Ni^{II} is metal exchange also possible at 80 °C, leading to almost complete substitution of peripheral Zn centers (Figure 2). However, analytically pure products, as determined by elemental analyses, were only obtained at 60 °C. Figure 2 shows that 50 % of the peripheral Zn^{2+} ions are substituted easily when an approximately equimolar M/Zn starting ratio is used. Further increase of the initial M/Zn ratio then results only in a moderate enhancement of the metal substitution degree. For this reason, we have used

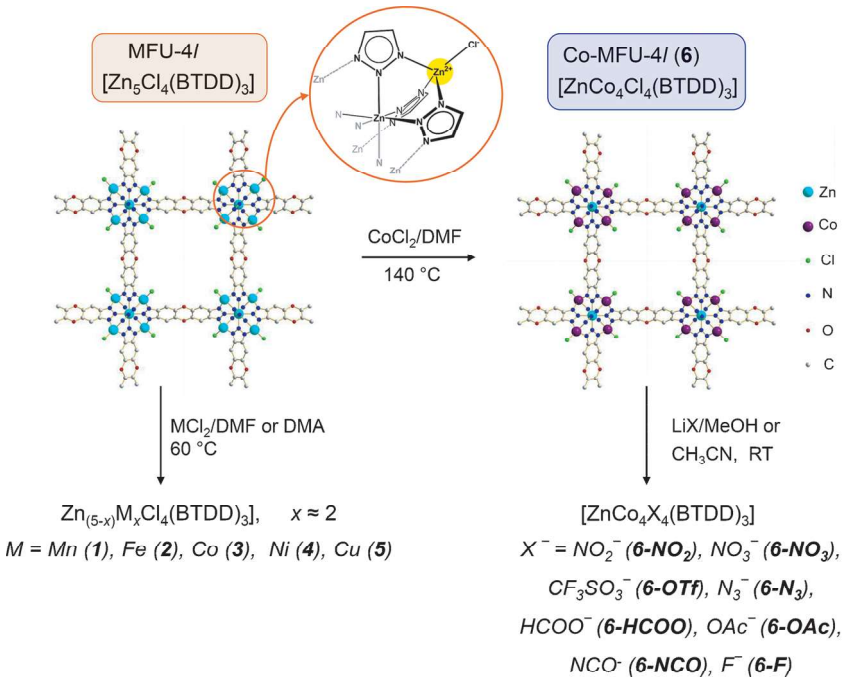

Scheme 1. Post-synthetic modifications of MFU-4*l* described in this study (DMF = *N*,*N*-dimethylformamide, DMA = *N*,*N*-dimethylacetamide).

a 13-fold excess of metal(II) chloride in 0.25 M DMA or DMF solution in preparative scale metal exchange procedures. Higher metal salt concentrations result in the precipitation of metal salts and should be avoided. To improve the metal substitution degree, samples of metal-exchanged MFU-4*l* have been subjected to a second exchange step employing identical starting conditions. However, according to analytical results, this second exchange did not improve the substitution degree significantly. For instance, in the case of Cu, the Zn/Cu exchange degree increased from 55 to 60% upon repeating the procedure. All MFU-4*l* hetero-metal derivatives thus prepared possess a thermal stability similar to the original MFU-4*l* framework (up to 400 °C according to TGA data, see the Supporting Information, Figure S1). XRPD data show that all derivatives are phase-pure and have the same structure as the parent framework MFU-4*l* (the Supporting Information, Figure S78). Also, the IR spectra are nearly identical to that of MFU-4*l* (the Supporting Information, Figures S10–S13). All frameworks are highly porous, as confirmed by argon sorption at 87.3 K (the Supporting Information, Figure S33). Our attempts to introduce other metal ions such as Ag^{+}, Pd^{2+}, or VO^{2+} into MFU-4*l* by using a similar procedure were unsuccessful up to now. Post-synthetic metal exchange in MFU-4*l* can be augmented by the side-ligand exchange reaction as exemplified for chloride exchange in Co-MFU-4*l* (Scheme 1). Hence, the chloride side-ligand can be substituted by a number of different anions such as NO_2^{-}, NO_3^{-}, N_3^{-}, $CF_3SO_3^{-}$, NCO^{-}, $HCOO^{-}$, CH_3COO^{-}, or F^{-}. Lithium salts well-soluble in methanol or acetonitrile were used in all cases except fluoride, in which case CsF soluble in methanol was applied. For weakly coordinating ligands (formate, acetate, nitrate, and triflate) a 20-fold excess of lithium salt in methanol was employed. In the case of triflate, the exchange with this procedure is incomplete. However, nearly 90% of chloride ligands can be substituted when the procedure is repeated twice. The success of ligand exchange was controlled mainly by EDX analysis and in several cases by FIR spectroscopy. Thus, a characteristic band at 383 cm^{-1} assigned to the Co–Cl stretch mode,[14] disappears almost completely upon side-ligand exchange (the Supporting Information, Figure S21). In the case of stronger coordinating ligands (nitrite, azide, and isocyanate), such large excess of lithium salt leads to discernible leaching of Co^{2+} ions from Co-MFU-4*l* (**6**) and to decomposition of the framework. For this reason, only a moderate excess of the corresponding lithium salt (≈25%) was used. Acetonitrile approved to be a better choice for these ligands leading to products with higher crystallinity. All attempts to introduce cyanide into Co-MFU-4*l* (**6**) failed completely due to immediate decomposition of the framework. Also, treatment with hydroxide led to decomposition of the framework, as verified by XRPD measurements. Fluoride exchange proceeds smoothly on all 3d transition-metal centers studied except zinc. Treatment of MFU-4*l* with CsF in methanol does not lead to the Cl/F exchange, as verified by EDX and IR measurements. EDX analyses show that partially substituted fluoride derivatives of Mn-, Fe-, Ni-, and Cu-MFU-4*l* (**1-F**, **2-F**, **4-F**, and **5-F**, respectively) contain a considerable amount of chloride, which corresponds well to a number of peripheral Zn^{2+} ions in the SBU and indicates that chloride side-ligands at Zn^{II} centers are not substituted by fluoride. Co-MFU-4*l*-fluoride (**6-F**) is, in contrast, almost chloride-free, since all four peripheral zinc ions in each SBU are replaced by Co^{II} centers in peripheral positions. According to the TGA data, all derivatives obtained after the side-ligand exchange are quite stable (at least up to 150 °C, see the Supporting Information, Figures S2, S3, and S6). XRPD measurements confirm phase purity and intact structure of the frameworks (the Supporting Information, Figures S79–81). The high porosity typical for MFU-4*l* frameworks is also retained (the Supporting Information, Figures S33 and S34).

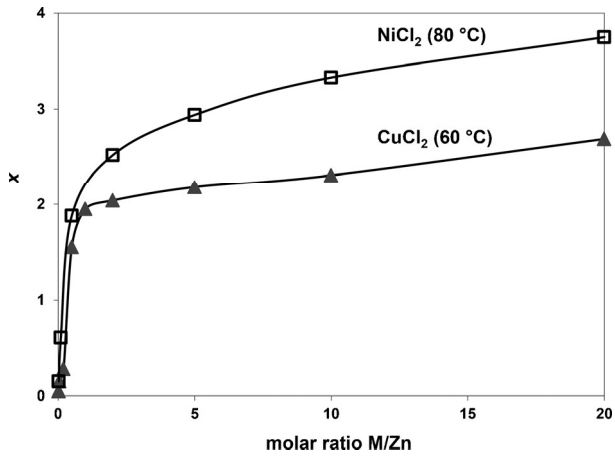

Figure 2. Total number, *x*, of Ni^{II} or Cu^{II} ions per $\{M_xZn_{5-x}Cl_4\}^{6+}$ unit as a function of (M/Zn) molar ratio in the starting reaction mixture (DMA, 20 h).

UV/Vis-NIR spectra

All derivatives except Mn-MFU-4*l* (**1**) show several absorption bands in the UV/Vis-NIR spectrum relating to d–d metal-centered valence electron transitions. Fe-MFU-4*l* (**2**) does not show any bands in the visible range, but it shows a strong charge-transfer (CT) band at 335 nm and other bands in the NIR range at 1385 and approximately 1660 nm (Figure 3).

The bands in the NIR range correspond to a split $^5T_2 \rightarrow {}^5E$ transition.[24] The tetrahedral complex $[FeQ_2Cl_2]$ (Q = quinuclidine) shows the same split band with two maxima at approximately 1400 and 1950 nm. The shift towards lower energy is caused by a weaker ligand field.[25] Ni-MFU-4*l* (**4**), when filled with DMA, is green-colored and shows bands at 630 and 1039 nm, which are typical for octahedral Ni^{II} ions and correspond to the $^3A_{2g} \rightarrow {}^3T_{1g}$ and $^3A_{2g} \rightarrow {}^3T_{2g}$ transitions, respectively.[24] The third spin-allowed transition, $^3A_{2g} \rightarrow {}^3T_{1g}(P)$, which normally appears at 370–520 nm, is overlapped by the strong ligand absorption and can hardly be seen as a shoulder at approximately 420 nm (Figure 4).

After solvent removal, compound **4** becomes red-colored. The tetrahedrally coordinated Ni^{II} ions with C_{3v}-symmetric ligand surrounding in **4** show a much more complicated spectrum (Figure 4), which has previously been observed for a similar scorpionate complex [Tp*NiCl] (Tp* = hydrotris(3,5-dimethyl-1-pyrazolyl)borate).[26] Thus, based on ligand-field calculations performed for [Tp*NiCl], the observed absorption bands

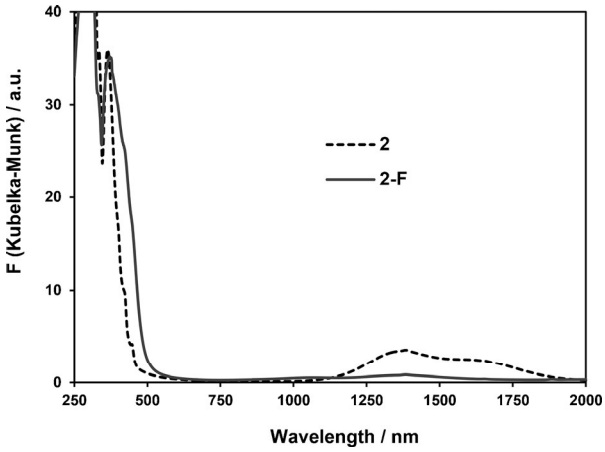

Figure 3. Diffuse reflectance UV/Vis-NIR spectra of **2** and **2-F**.

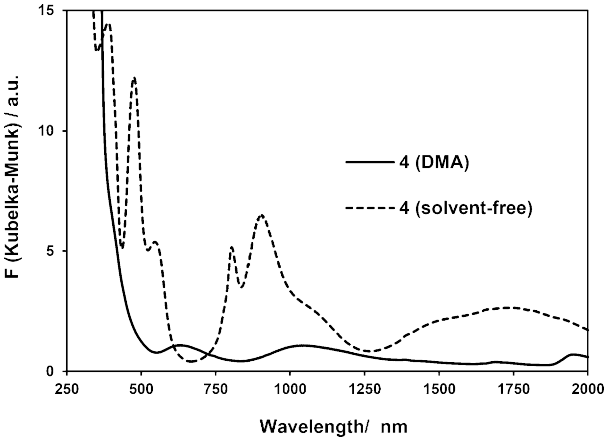

Figure 4. Diffuse reflectance UV/Vis-NIR spectra of **4** (filled with DMA and solvent-free).

can be assigned as the following transitions: 386 nm: CT, 475 nm: $^3A_2(^3T_1, F)\rightarrow{}^3A_2(^3A_2, F)$, 547 nm: $^3A_2(^3T_1, F)\rightarrow{}^3E(^3T_1, P)$, 804 nm: $^3A_2(^3T_1, F)\rightarrow{}^3A_2(^3T_1, P)$, 905 nm: $^3A_2(^3T_1, F)\rightarrow{}^3E(^3T_2, F)$, 1743 nm: $^3A_2(^3T_1, F)\rightarrow{}^3E(^3T_1, F)$. The same behavior was observed in case of Cu^{II}-MFU-4*l* (**5**): When filled with DMA, the compound is green and shows absorption bands typical for sixfold coordinated Cu^{II}. Solvent-free **5** is red–brown and shows very intensive absorption bands at 417, 523, and 997 nm (Figure 5).[15]

These spectral features are very similar to previously described scorpionate complexes [$Tp^{tBu,Me}$CuCl] and [Cu(L)Cl]-(CLO_4), in which $Tp^{tBu,Me}$ = hydrotris(3-*tert*-butyl-5-methyl-1-pyrazolyl)borate and L = tris(3-*tert*-butyl-5-methyl-1-pyrazolyl)methane.[27] Thus, the first two bands at 417 and 523 nm can be assigned to the Cl^- to Cu^{II} CT transitions, the third one at 997 nm to the d–d transition at the Cu^{II} centers. In **5-F**, the CT absorption bands disappear almost completely, which remains in agreement with the much higher electronegativity of fluorine. At the same time, also the intensities of d–d transitions become much lower (Figure 5). The same behavior is observed

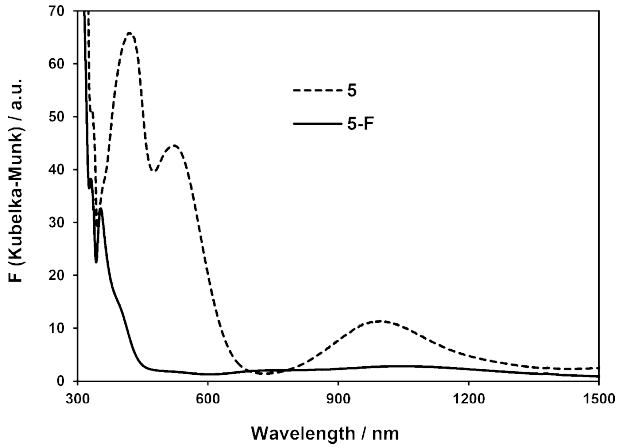

Figure 5. Diffuse reflectance UV/Vis-NIR spectra of **5** and **5-F**.

for **4-F** (the Supporting information, Figure S9). In **2-F**, only the intensity of the d–d transitions is reduced, whereas the intensity of the CT band remains unchanged (Figure 3). This can be explained by the nature of the transition, which is in this case most probably metal-to-ligand charge-transfer involving a triazolate moiety. In contrast, such a hypochromic effect is not observed for **6-F** (the Supporting Information, Figure S8). These phenomena are well known in coordination chemistry, but have no simple explanation. Qualitatively, the intensity of a d–d transition grows with increasing covalency of a metal–ligand bond and respective mixing between metal and ligand orbitals.[24] The fluoride ligand has a much higher ionic character compared with chloride, and thus leads to low intensities of d–d transitions. The spectral properties of Co-MFU-4*l* (**6**) described previously[14] undergo strong changes upon substitution of chloride ligands. UV/Vis-NIR spectra of selected derivatives of **6** are shown on Figure 6. Substitution of the chloride ligand by azide leads to a very intensive CT absorption band at 389 nm. The strong absorption band centered at 612 nm, typical for tetrahedral Co^{II} ions, is more intense and shows a much stronger split compared with **6**. Framework **6-HCOO** contains fivefold coordinated Co^{II} ions, which results in a significant shift and much lower intensity of the absorption bands. Figure S8 (the Supporting information) shows that nitrite, nitrate, and triflate derivatives of **6** also contain fivefold coordinated Co^{II}, as confirmed by comparison to the literature-known complex [Tp*Co(OAc)].[28] Nitrite is an interesting case since it is known to coordinate either in monodentate (nitro-, by the N-atom) or bidentate (nitrito-, by two oxygen atoms) fashion. The nitrito-to-nitro linkage isomerization has been extensively studied for Co^{III}[29] and it has been found that the nitro-form is more stable.[30] However, in the case of scorpionate-type coordination of Co^{II}, the nitrito-form seems to be more stable. Thus, [$Tp^{tBu,Me}Co(NO_2)$] contains fivefold coordinated Co^{II} with the nitrite ligand coordinated by two oxygen atoms.[31] [$Tp^{Ph_2}Co(NO_2)$] (Tp^{Ph_2} = hydrotris(3,5-diphenyl-1-pyrazolyl)borate) shows complex solution behavior being blue (tetrahedrally coordinated) in CH_2Cl_2 and pink-red (fivefold coordinated) in THF.[32]

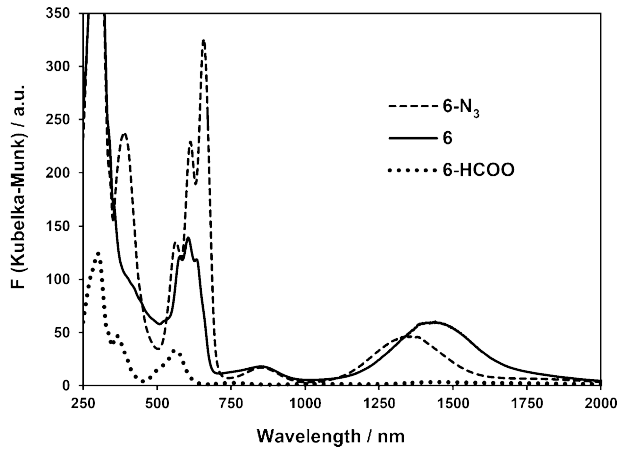

Figure 6. Diffuse reflectance UV/Vis-NIR spectra of selected derivatives of **6**.

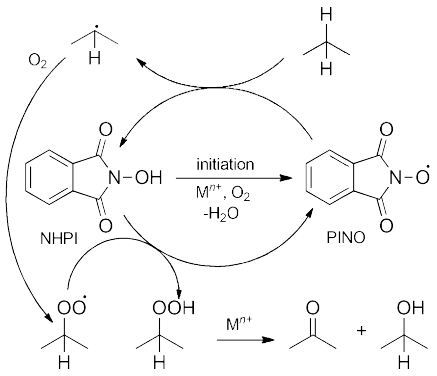

Scheme 2. Schematic representation of the aerobic oxidation of hydrocarbons catalyzed by the NHPI/PINO system in the presence of transition-metal ions.

Liquid-phase aerobic oxidation

MFU-4*l* frameworks featuring coordinatively unsaturated metal sites, large pores, and high thermal stability are promising candidates for catalytic applications. Binding of the O_2 molecule at the active metal site is a crucial step for the gas-phase oxidation under mild conditions. Searching for MOFs that could be utilized for heterogeneously catalyzed reactions employing molecular oxygen, we have systematically studied heterometallic MFU-4*l* derivatives. Since physisorption enthalpies for argon and oxygen are very similar,[33] a comparison of the isosteric heats of Ar and O_2 adsorption will show whether chemisorptive oxygen binding at the unsaturated metal site takes place or not. Unfortunately, in all tested cases, the heats of Ar and O_2 adsorption determined from the adsorption isotherms measured in the temperature range 183–213 K (as described in the Supporting information, pp. S13–S31), are very similar (Table S1). Density-functional theory (DFT) calculations of O_2 binding energies on metal centers in scorpionate-type coordination, which was used as a model environment for metal sites in MFU-4*l*, confirm these results and show that strongly basic ligands such as hydroxide, hydride, or amide would enable oxygen binding.[34] Only in these cases was sufficient charge transfer from the metal center to the oxygen identified through Hirshfeld charge analyses. Unfortunately, up to now, we were not able to prepare these derivatives. It seems that tetrahedral and fivefold coordination of divalent metal centers in MFU-4*l* frameworks comprising one additional side ligand is less favorable for binding small molecules if compared with Cu^{I}-MFU-4*l* featuring trigonal-pyramidal Cu^{I} sites and showing quite strong O_2 binding.[15] Although MFU-4*l* derivatives seem rather inactive in terms of dioxygen binding from the gas phase, they show catalytic activity in liquid-phase oxidation reactions. Selective oxidation of hydrocarbons is an important process for fine chemical synthesis. MOFs have been extensively tested as catalysts for this kind of application. In most cases, different peroxides such as H_2O_2 or *t*BuOOH were applied as oxidizing agents.[4d] Molecular oxygen is the most attractive oxidant due to its unlimited availability. However, due to its low reactivity at low temperatures, oxygen activation still remains a challenge. One effective strategy for oxygen activation is the use of *N*-hydroxyphthalimide (NHPI) as co-catalyst, which is easily oxidized to phthalimide *N*-oxyl radical (PINO) with air in the presence of transition-metal ions. PINO acts then as initiator for the radical oxidation of C—H bonds (Scheme 2).[35]

This strategy has been successfully applied with homogeneous catalysts such as acetates or acetylacetonates of V^{IV}, Mo^{VI}, Mn^{III}, Fe^{III}, Co^{II}, Co^{III}, and Cu^{II}.[36] Several MOFs have been tested as catalysts for this reaction. Thus, MFU-1 was found to be catalytically active in the PINO-mediated oxidation of cyclohexanol, cyclohexane, cyclohexene, and ethylbenzene.[37] Solution impregnation of MFU-1 with NHPI led to a heterogeneous catalyst NHPI@MFU-1 suitable for solvent-free oxidation of hydrocarbons. Similar catalytic model reactions have been reported subsequently for Fe-BTC[38] and Co-BTT.[39] Continuing our work on MFU-1 derivatives we have tested different MFU-4*l* derivatives as catalysts in the aerobic oxidation of ethylbenzene under mild reaction conditions (Scheme 3).

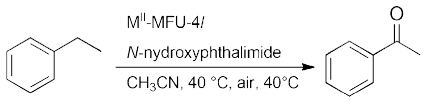

Scheme 3. Liquid-phase oxidation of ethylbenzene. Reaction conditions: catalyst (1 mol % based on Mn-, Fe-, Co-, Ni- or Cu centers), NHPI (10 mol %).

The results are summarized in Table 1. The highest conversion is achieved with **5**, **6**, and **6-OAc** (within the experimental error). Even though **5** remains highly crystalline (the Supporting information, Figure S82) and porous (BET surface area 3232 $m^2 g^{-1}$, as determined by N_2 sorption at 77.3 K) after the reaction, the hot filtration test, performed after 24 h reaction time, shows probable leaching of Cu^{2+} ions.

The conversion in filtered solution increases with time in a similar way as in the unfiltered reaction mixture (Figure 7, △). A prolonged induction period indicates the slow formation of PINO radicals in the beginning and could also indicate the leaching of Cu^{2+} ions. However, the amount of leached Cu^{2+} ions must be very low since EDX analysis of **5** recovered after catalysis shows an unchanged Zn/Cu ratio (see the Experimen-

Table 1. Conversions and selectivities for the liquid-phase oxidation of ethylbenzene catalyzed by MFU-4*l* derivatives after a reaction time of 48 h.

Compound	Metal ion	Side ligand	Conversion of ethylbenzene [%]	Selectivity ketone/alcohol[a]
6	Co^{2+}	Cl^-	27±3	97
6-OAc	Co^{2+}	CH_3COO^-	26±3	95
6-NO$_3$	Co^{2+}	NO_3^-	8±1	95
6-OTf	Co^{2+}	$CF_3SO_3^-$	3±0.5	–
1	Mn^{2+}	Cl^-	0	–
2	Fe^{2+}	Cl^-	0	–
4	Ni^{2+}	Cl^-	9±1	–
5	Cu^{2+}	Cl^-	28±3	95

[a] The selectivity for **4** and **6-OTf** could not be estimated due to very low content of alcohol

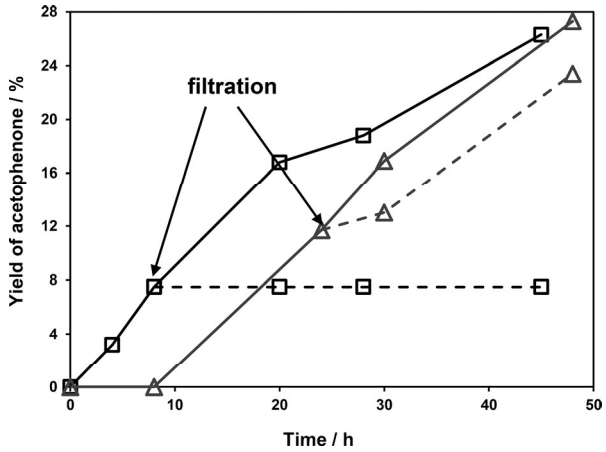

Figure 7. Time-dependent formation of acetophenone in the PINO-mediated oxidation of ethylbenzene catalyzed by **5** (△) and **6** (□). Dashed lines show the reaction progress after hot filtration.

tal Section). In contrast, framework **6**, having nearly the same activity, does not show such an induction period. The heterogeneous character of catalysis is confirmed by the hot filtration test performed after 8 h reaction time (Figure 7, □). Framework **6** also remains stable after the reaction, but the crystallinity (the Supporting information, Figure S83) and porosity (BET surface area 2172 $m^2 g^{-1}$, as determined by N_2 sorption at 77.3 K) become slightly decreased. The EDX analysis of **6** recovered after catalysis shows, similarly to **5**, an unchanged Zn/Co ratio (see the Experimental Section). Framework **6-OAc** shows almost the same activity, whereas **6-NO$_3$** and **6-OTf** are much less active. Framework **4** shows low activity, as compared with that of **5** and **6**. Frameworks **1** and **2** are not stable under reaction conditions: A fast oxidation of Mn^{2+} or Fe^{2+} ions and no conversion of ethylbenzene were observed. GC/MS analysis shows the formation of 1-phenylethanol as a byproduct in all cases (the Supporting information, Figure S76). However, the ketone/alcohol selectivity is very high (≥95%) in all cases. In general, framework **6** shows similar activity and selectivity as MFU-1. Interestingly, only traces of benzoic acid (<0.1%) were found in the reaction mixture as revealed by ESI-MS analysis (for details see the Supporting information, pp. S33–S34). The recyclability test shows that **6** recovered after catalysis has almost unchanged activity and gives 25.7% conversion in the second run, which is 94% of the value listed in Table 1.

Thermal transformations of MFU-4*l*-formates and azides

As shown by us in a recent report, the thermal decomposition of formate moieties at peripheral Zn^{II} centers in MFU-4*l*-HCOO leads to the formation of Zn–H species, whereas decomposition of Cu^{II}-HCOO moieties gives Cu^{I} species.[15] Thus, thermal decomposition of formate ligands can be considered as a method for the in situ generation of reactive or low-valent metal sites. TGA measurements show that formate side-ligands at the peripheral 3d transition-metal sites in heterometallic derivatives of MFU-4*l* can be selectively decomposed, as can be seen by the stability range without weight loss, before the decomposition of the framework starts (the Supporting information, Figure S3). Only in the case of **6-HCOO** is the stability range less well pronounced. Table 2 shows decomposition ranges of formate ligands at different metal(II) centers in hetero-metal derivatives of MFU-4*l* determined by TGA.

Table 2. Temperatures for thermal transformations of formate side-ligands in heterometallic derivatives of MFU-4*l*.[a]

Compound	Metal ion	Start [°C]	End [°C]
MFU-4*l*-HCOO	Zn^{2+}	195	280
1-HCOO	Mn^{2+}	330	370
2-HCOO	Fe^{2+}	195	325
6-HCOO	Co^{2+}	195	325
4-HCOO	Ni^{2+}	180	280
5-HCOO	Cu^{2+}	120	180

[a] Determined by TGA under N_2 flow with a heating rate of 5 K min^{-1}.

It has to be noted that only Zn- and Co-MFU-4*l*-formates contain only one type of peripheral metal ions; the other derivatives are mixed with zinc. In the case of Mn^{II} and Cu^{II}, the decomposition steps are well separated, since Cu-HCOO moieties decompose at considerably lower, and Mn-HCOO at considerably higher temperature, than Zn-HCOO. XRPD measurements show that the crystallinity of **2-HCOO** and **4-HCOO** is completely retained after decomposition of formate side-ligands (the Supporting information Figure S84). The crystallinity of **6-HCOO** becomes lower and **1-HCOO** shows only main X-ray reflexes after thermal treatment. Treatment of **6-HCOO** under CO gas flow at 325 °C gives a proof for the formation of low-valent cobalt sites (Scheme 4). Thus, a band appearing at 1971 cm^{-1} (the Supporting information, Figure S30) is very similar to a CO stretch in Co^{I}-containing scorpionate [$Tp^{iPr,Me}$Co(CO)] (1940 cm^{-1}, $Tp^{iPr,Me}$ = hydrotris(3-isopropyl-5-methyl-1-pyrazolyl)borate).[40]

The DFT-calculated CO stretching frequency for the scorpionate Co^{I}-CO cluster is 1966 cm^{-1}. Further detailed studies on thermal transformations of formate side-ligands in heterometallic derivatives of MFU-4*l* have to be performed to explore the potential of this strategy for the generation of highly

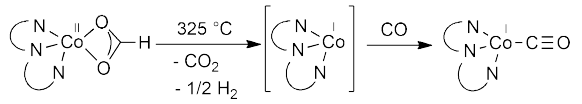

Scheme 4. Schematic representation for the formation of Co^{I}–CO species after thermal treatment of **6-HCOO** under CO gas flow.

active metal sites. Another interesting reaction is a thermal transformation of azide to isocyanate under CO gas in **6**. The reaction is very clean, as confirmed by IR spectroscopy (Figure 8) and most likely involves a nitrene as an intermediate. The crystallinity of the product is somewhat lower, compared with that of **6-N$_3$** and **6-NCO** prepared through the side-ligand exchange, but all X-ray reflexes are retained and no impurities can be seen (the Supporting Information, Figure S85).

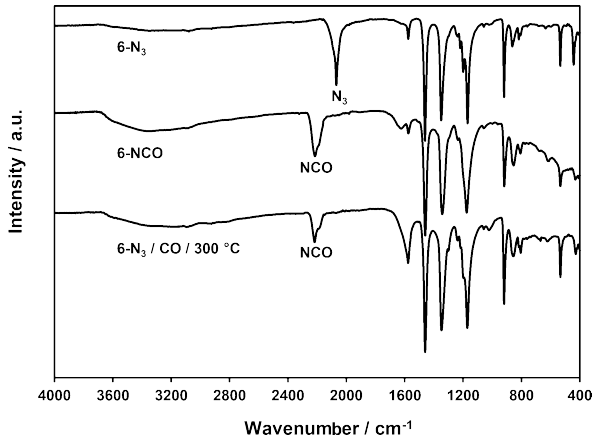

Figure 8. IR spectra of **6-N$_3$**, **6-NCO** (prepared form **6** by ligand exchange), and of the product obtained from **6-N$_3$** after heating under CO flow at 300 °C.

Transition-metal nitrene (nitrido- or imido-) complexes[41] have attracted much attention due to their supposed role in biological nitrogen fixation[42] and potential as N-atom transfer reagents.[43] Aryl-substituted bis(imino)pyridine cobalt azide complexes (^{iPr}BPDI)CoN$_3$ and (^{Mes}BPDI)CoN$_3$ have been shown to generate a nitrene intermediate under photolytic or thermal (215 °C) conditions, which then undergoes an intramolecular insertion into the C–H bond.[44] (^{Mes}BPDI)CoN$_3$ reacts with CO in toluene at 23 °C to give (^{Mes}BPDI)CoNCO. These mild conditions for the reaction with CO, in contrast to the intramolecular insertion into the C–H bond, indicate that the latter transformation proceeds more likely through the direct insertion of the CO molecule into azide. The solvent-assisted conversion of coordinated azide anions to isocyanate ligands under mild conditions has also been described in several other cases.[45] The conversion of **6-N$_3$** to **6-NCO** does not occur at RT and thus most probably involves the formation of a nitrene intermediate representing heterogeneous single-site reaction (Scheme 5). According to DFT calculations, the formation of a nitrene in the first step is endothermic (127 kJ mol^{-1}) with an activation energy of 217 kJ mol^{-1}. The barrier occurs at the Co–N···N$_2$ distance of 1.7 Å. Subsequent reaction with CO to isocyanate

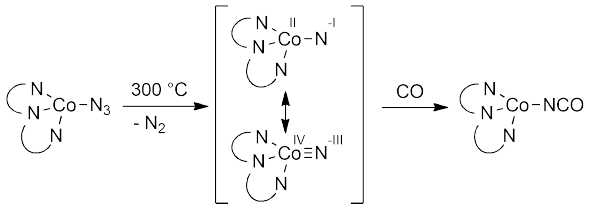

Scheme 5. Schematic representation of the conversion of **6-N$_3$** to **6-NCO** through the nitrene intermediate.

takes place spontaneously without any barrier and is highly exothermic (−380 kJ mol^{-1}).

Preparation of Cu^{I}-MFU-4*l* in different ways

Previously, we have described the preparation of Cu^{I}-MFU-4*l* through the thermolysis of **5-HCOO** (path **d** in Scheme 6).[15] Using the possibilities for the postsynthetic modification of MFU-4*l*, Cu^{I} centers can be generated also in alternative ways. Thus, heating a suspension of **5** in DMF at 140 °C leads to a colorless product (path **a** in Scheme 6). The presence of Cu^{I} centers in this product is confirmed by oxygen adsorption isotherms showing clear chemisorption (the Supporting Information, Figure S46, left). The heat of oxygen chemisorption (50 kJ mol^{-1}, the Supporting Information, Figure S75) is very close to the one previously described for Cu^{I}-MFU-4*l* (52 kJ mol^{-1}).[15] Additionally, the formation of Cu^{I} centers is supported by the IR spectrum after CO adsorption (the Supporting Information, Figure S31): A characteristic CO stretch at 2090 cm^{-1} is observed (2081 cm^{-1} in a previously described Cu^{I}-MFU-4*l* prepared through path **d**). However, the amount of chemisorbed oxygen (≈10 cm^3 g^{-1}, as seen from the adsorption isotherms) is much lower as described previously (38 cm^3 g^{-1}). Also, a small deviation in the heat of oxygen adsorption and position of the CO stretch as well as significantly reduced BET surface area (2615 m^2 g^{-1}) indicate that the reaction is not clean. The mechanism probably includes the formation and further decomposition of Cu-formate moieties (formate is produced by the hydrolysis of DMF). Path **b** on Scheme 6 shows a direct substitution of Zn^{2+} centers by Cu^{I} in MFU-4*l*. Since CuCl is not soluble in common solvents (except strongly coordinating solvents such as pyridine), we added lithium chloride, which leads to the formation of a mixture of soluble chloro cuprates(I). The product obtained in this way shows the same oxygen chemisorption with the heat of 52 kJ mol^{-1} (the Supporting Information, Figures S46 and S75), which matches exactly the value described previously. However, the amount of chemisorbed oxygen (≈12 cm^3 g^{-1}) is also very low, due to much lower exchange degree. Both products, prepared through the pathways **a** and **b** (Scheme 6), show the same high crystallinity as **5** (the Supporting Information, Figure S86). Finally, Cu^{I} centers in MFU-4*l* can be generated by the gas-phase reaction of **5-F** with H$_2$ at 240 °C (path **c** on Scheme 6).

Thus, the TGA curve of **5-F** under H$_2$/Ar flow shows a weight loss in the range 120–220 °C, which is not observed under N$_2$

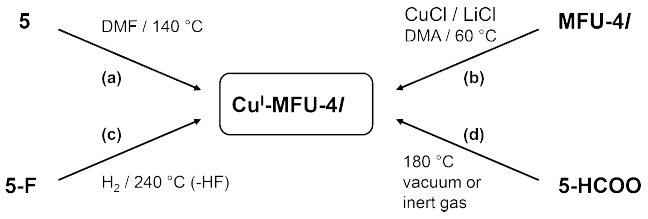

Scheme 6. Different ways for the preparation of Cu^{I}-MFU-4*l*.

(Figure 9). The weight loss of 2.8% corresponds well to the loss of fluoride ligands connected to Cu^{II} centers (calcd 3.1%). The product obtained in this way shows typical oxygen chemisorption with the heat of adsorption of 52 kJ mol^{-1} (the Supporting Information, Figures S47 and S75). The chemisorbed amount of approximately 34 cm^3 g^{-1}, high porosity (BET surface area 3682 m^2 g^{-1}), crystallinity (the Supporting Information, Figure S87) and the results of the elemental analysis confirm the purity of the obtained product with the formula [$Cu_2Zn_3Cl_2(BTDD)_3$]. Interestingly, framework **5** exhibits a similar weight loss of 4.9% in the range 250–350 °C under H_2/Ar flow, as indicated by the TGA curve (the Supporting Information, Figure S4). This weight loss corresponds quite well to the loss of two chloride ligands at the Cu^{II} centers (calcd 5.6%) and could be assumed as a formation of Cu^{I} centers. Formation of HCl in the gas phase was confirmed by TG/MS measurement (the Supporting Information, Figure S5). The loss of halide seems to occur at higher temperature even under nitrogen. Thus, both frameworks **5** and **5-F** show a weight loss in the range 350–400 °C (Figure 9 and the Supporting Information, Figure S4) before the decomposition of the framework starts.

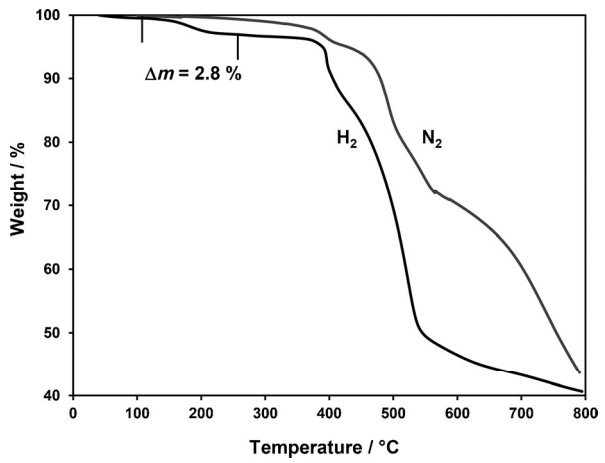

Figure 9. TGA curves for **5-F** under N_2 and H_2/Ar (1:9) flow.

Oxygen adsorption isotherms for products, obtained from **5** by heating at 350 °C under H_2/Ar flow or 400 °C under N_2 flow, show clearly that no chemisorption occurs and thus both products do not contain active Cu^{I} sites (the Supporting Information, Figure S47, right). Although the crystallinity in both cases is retained (only two small additional reflexes at 6.8 and 7.4° 2θ are observed, the Supporting Information, Figure S87), the porosity is strongly reduced to 2078 and 2054 m^2 g^{-1}, respectively. The results of the elemental analysis are similar in both cases and give C/N ratios of 36:16.6 and 36:16.1, respectively, whereas an ideal ratio for an unchanged MFU-4*l* framework must be 36:18. This indicates clearly that the triazolate moieties lose some nitrogen atoms and partial decomposition of the framework occurs under these conditions. Thus, only the reduction of **5-F** with hydrogen under milder conditions represents an alternative way for the preparation of pure Cu^{I}-MFU-4*l*. TGA studies on other fluoride derivatives of MFU-4*l* show that no reaction with H_2 takes place before the framework starts to decompose (the Supporting Information, Figure S6). The mechanism of the reaction of Cu^{II}-fluoride units in **5-F** with hydrogen probably proceeds through a heterolytic cleavage of the H_2 molecule followed by the decomposition of a Cu^{II}-hydride intermediate (Scheme 7).

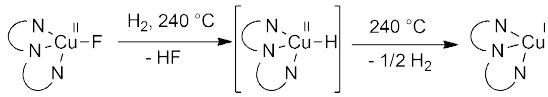

Scheme 7. Schematic representation of the conversion of Cu^{II}-F units to Cu^{I} in **5-F** through the Cu^{II}–H intermediate.

Fluoride ligands serve as basic anions forming very stable H–F bonds and thus driving the reaction. According to our DFT calculations, the formation of Cu^{II}–H species in the first step is endothermic (44 kJ mol^{-1}) with an activation energy of 80 kJ mol^{-1}. The barrier occurs at a Cu–F···H_2 distance of 1.2 Å and at that distance the H···H bond is elongated to 1.02 Å (normal bond length for H_2 molecule is 0.74 Å). Subsequent dissociation of Cu^{II}-hydride species to Cu^{I} and H radicals (which then recombine to H_2 molecules) has a calculated activation energy of 145 kJ mol^{-1} and the full free radical split takes place at a Cu···H distance of approximately 3 Å. Heterolysis of the H_2 molecule by Cu^{I} *tert*-butoxide in the presence of phosphine ligands in a THF solution leading to a hexameric Cu^{I}-hydride complex has been described.[46] This complex was shown to reduce α,β-unsaturated carbonyl compounds with high yields and selectivities.[47] Heterolytic cleavage of hydrogen was also observed, for instance, for a Fe^{II} complex that served as a model for the hydrogenase enzyme,[48] as well as for some other transition-metal ions such as Co^{II}, Mn^{I}, Mo^{III}, Re^{I}, Ru^{I}, Ir^{II}, Pd^{II}, and Pt^{II}.[49] To the best of our knowledge, the heterogeneous reaction of **5-F** with hydrogen represents the first example for the heterolytic cleavage of a H_2 molecule on single-site active centers within a metal–organic framework.

Conclusion

Post-synthetic metal and side-ligand exchange reactions enable the preparation of a large variety of MFU-4*l* derivatives with the general formula [$M_xZn_{(5-x)}(L)_yCl_{(4-y)}(BTDD)_3$], in which M = Mn^{II}, Fe^{II}, Co^{II}, Ni^{II}, Cu^{II}, and L = NO_2^-, NO_3^-, $CF_3SO_3^-$, N_3^-, NCO^-, $HCOO^-$, CH_3COO^-, and F^-. The possibilities and limitations of this approach are shown in the manuscript. Several of

thus-prepared MFU-4*l* derivatives show high catalytic activity in a liquid-phase oxidation of ethylbenzene to acetophenone with air under mild conditions, among which Co- and Cu derivatives with chloride side-ligands are the most active. Further thermal transformations of the side ligands in the gas phase, such as the decomposition of formate, conversion of azide to isocyanate, and removal of fluoride can be performed selectively without destroying the framework. Thermal conversion of Co^{II}-azide units in the SBU of Co-MFU-4*l* involves the formation of a nitrene intermediate, which is potentially interesting as an N-atom transfer reagent. Treatment of Cu^{II}-fluoride units with H_2 at 240 °C leads to Cu^{I} and proceeds through the heterolytic cleavage of the H_2 molecule, showing the potential of Cu^{II}-MFU-4*l*-fluoride as a catalyst for hydrogenation reactions. Thus, combined with its robustness, the MFU-4*l* family represents a modular "construction kit", which allows fine adjustments of the framework properties and can be suggested for different applications such as catalysis, sensing, gas capture, storage, and separation. Further studies on MFU-4*l* derivatives should be highly rewarding in terms of searching for new functional porous materials.

Experimental Section

General procedures

All starting materials were of reagent grade and used as received from the commercial supplier. [Tp*Co(OAc)] was prepared according to the literature procedure.[28] Fourier transform infrared (FTIR) spectra were recorded with an ATR unit in the range 4000–180 cm^{-1} on a Bruker Equinox 55 FTIR spectrometer. Diffuse reflectance UV/Vis-NIR spectra were recorded in the range 2000–250 nm on a PerkinElmer λ 750 s spectrometer equipped with a Labsphere 60 mm RSA ASSY integrating sphere with 0°/d measuring geometry. Labsphere Spectralon SRS-99 was used as a white standard. Thermogravimetric analyses (TGA) were performed with a TA Instruments Q500 analyzer in the temperature range of 25–900 °C in flowing nitrogen gas at the heating rate of 5 K min^{-1}. TG/MS measurements were performed with the same instrument combined with the Hiden QIC-20 gas analysis system. Energy-dispersive X-ray spectroscopy (EDX) was performed with a Philips XL 30 scanning electron microscope. An area of at least 10×10 μm including at least 10 MOF crystals was scanned. Elemental analyses were measured with a Vario EL III instrument from Elementar Analysensysteme GmbH. GC/MS measurements were performed on a Hewlett Packard GC System 6890 Series equipped with Rtx-5MS column and mass selective detector MSD 5973. N_2 adsorption isotherms for the determination of BET surface areas were measured at 77 K in the relative pressure range 0.01–0.45 with a Quantachrome NOVA 2000 Series instrument. O_2 and Ar adsorption isotherms were measured with a BELSORP-max instrument combined with a BELCryo system. Adsorbed amounts are given in $cm^3 g^{-1}$ [STP], in which STP = 101.3 kPa and 273.15 K. Powder X-ray diffraction data were collected in the 2θ range of 4–70° with 0.02° steps, with a time of 200 s per step, by using a Seifert XRD 3003 TT diffractometer equipped with Meteor 1D detector. All DFT calculations have been performed with the all-electron full-potential code FHI-aims.[50] Electronic exchange and correlation was treated on the level of the generalized gradient approximation (GGA) PBE functional[51] for the geometry optimizations and on the level of the hybrid B3LYP functional[52] for consecutive single-point calculations on these optimized geometries. Dispersive interactions lacking at these levels of theory were considered through the dispersion-correction scheme according to Tkatchenko and Scheffler.[53] Geometry optimization was performed using tight, tier1 basis sets until residual forces fell below 10^{-4} eV $Å^{-1}$. Hybrid B3LYP + TS energetics are the finally presented numbers in the paper. Reaction barriers presented in the paper were obtained through calculations of the potential energy of the system going from initial to final state by having one constraint-fixed distance along the main reaction coordinate.

Syntheses

Preparation of lithium salts: A lithium formate solution in MeOH was prepared as described previously.[15] Methanolic solutions of $LiNO_2$, LiN_3, and LiNCO were prepared by the following general procedure: LiCl (4.24 g, 100 mmol) and $NaNO_2$, NaN_3 or NaNCO (115 mmol) were stirred under reflux in methanol (100 mL) for 16 h. After cooling to RT, the precipitate was filtered off and the resulting approximately 1 M methanolic solution of $LiNO_2$, LiN_3, or LiNCO was used for further transformations.

General procedure for the metal exchange in MFU-4*l*: Metal(II) chloride ($MnCl_2 \cdot 4H_2O$, $FeCl_2 \cdot 4H_2O$, $NiCl_2 \cdot 6H_2O$, $CoCl_2$ or $CuCl_2$, 32.5 mmol) was dissolved in *N*,*N*-dimethylformamide (for $FeCl_2$) or *N*,*N*-dimethylacetamide (130 mL) and MFU-4*l* (0.8 g, 0.634 mmol) was added to the solution. The reaction mixture was heated for 20 h at 60 °C in a sealed tube. In the case of $FeCl_2$, the reaction was performed at 50 °C under an Ar atmosphere. The precipitate was filtered off, washed with DMF or DMA, methanol and dichloromethane and dried at 150 °C under vacuum. The yield is close to quantitative. The number of M^{2+} ions in the formula unit was calculated from the M/Zn ratio determined by EDX analysis. All products are hygroscopic and may contain variable amounts of adsorbed water.

Mn_2-MFU-4*l* (1): Pale-yellow powder. Number of Mn^{2+} ions in the formula unit: 1.86; IR (ATR): $\tilde{\nu}$ = 3076 (w), 1577 (w), 1460 (s), 1349 (s), 1239 (w), 1218 (m), 1198 (m), 1170 (s), 919 (m), 869 (m), 816 (w), 531 (m), 428 cm^{-1} (w); BET surface area (Ar, 87.3 K): 3512 $m^2 g^{-1}$; elemental analysis calcd (%) for $C_{36}H_{12}Cl_4N_{18}O_6Mn_2Zn_3$: C 34.86, H 0.98, N 20.33; found: C 34.59, H 1.23, N 20.12.

Fe_2-MFU-4*l* (2): Yellow powder. Number of Fe^{2+} ions in the formula unit: 1.50; IR (ATR): $\tilde{\nu}$ = 3078 (w), 1577 (w), 1461 (s), 1351 (s), 1239 (w), 1219 (m), 1203 (m), 1174 (s), 920 (m), 869 (m), 817 (w), 532 (m), 429 cm^{-1} (w); UV/Vis-NIR: λ_{max} = 335, 1385 nm; BET surface area (Ar, 87.3 K): 3470 $m^2 g^{-1}$; elemental analysis calcd (%) for $C_{36}H_{12}Cl_4N_{18}O_6Fe_{1.5}Zn_{3.5}$: C 34.67; H 0.97; N 20.22; found: C 34.25; H 1.49; N 20.06.

Co_3-MFU-4*l* (3): Green-blue powder. Number of Co^{2+} ions in the formula unit: 3.13. IR (ATR): $\tilde{\nu}$ = 3078 (w), 1576 (w), 1460 (s), 1351 (s), 1239 (w), 1220 (m), 1204 (m), 1173 (s), 919 (m), 869 (m), 818 (w), 533 (m), 429 cm^{-1} (w); BET surface area (N_2, 77.3 K): 3639 $m^2 g^{-1}$; elemental analysis calcd (%) for $C_{36}H_{12}Cl_4N_{18}O_6Co_3Zn_2$: C 34.81, H 0.97, N 20.30; found: C 34.74, H 1.23, N 20.09.

Ni_2-MFU-4*l* (4): Red powder. Number of Ni^{2+} ions in the formula unit: 2.13. IR (ATR): $\tilde{\nu}$ = 3079 (w), 1576 (w), 1460 (s), 1350 (s), 1242 (w), 1212 (m), 1187 (s), 1062 (w), 920 (m), 869 (m), 808 (w), 535 (m), 429 cm^{-1} (w); UV/Vis-NIR, with DMA: λ_{max} = 630, 1039, 1952 nm; dry: λ_{max} = 386, 475, 547, 804, 905, 1743 nm; BET surface area (Ar, 87.3 K): 3290 $m^2 g^{-1}$; elemental analysis calcd (%) for $C_{36}H_{12}Cl_4N_{18}O_6Ni_2Zn_3 \cdot 2H_2O$: C 33.68, H 1.26, N 19.64; found: C 33.52, H 1.33, N 19.45.

General procedures for the side-ligand exchange in heterometallic MFU-4*l* derivatives: a) *Formates, acetates, nitrates, and tri-*

flates: MFU-4*l* derivative (150 mg, approx. 0.12 mmol) was stirred with 0.2 M solution of lithium salt (HCOOLi, LiOAc, $LiNO_3$, or LiOTf) in methanol (50 mL, 10 mmol) for 30 min at RT. The precipitate was filtered off, washed with methanol and CH_2Cl_2 and dried at 80 °C under vacuum. In the case of triflate, the exchange procedure was repeated twice. b) *Nitrites, azides and isocyanates*: 1 M solution of lithium salt ($LiNO_2$, LiN_3, or LiNCO) in methanol (0.6 mL, 0.6 mmol) was added to a suspension of MFU-4*l* derivative (150 mg, approx. 0.12 mmol) in acetonitrile (30 mL) and the mixture was stirred for 30 min at RT. The precipitate was filtered off, washed with methanol and CH_2Cl_2, and dried at 80 °C under vacuum. *c) Fluorides*: MFU-4*l* derivative (150 mg, approx. 0.12 mmol) was added to a solution of CsF (91 mg, 0.6 mmol) in methanol (30 mL) and the mixture was stirred for 30 min at RT. The precipitate was filtered off, washed with methanol and CH_2Cl_2, and dried at 150 °C under vacuum. The yield is in all cases close to quantitative. The substitution degree of chloride ligands was calculated from the Zn/M/Cl atomic ratio, determined by EDX analysis.

Co-MFU-4*l*-nitrite (6-NO_2): Purple powder. Zn/Co/Cl ratio: 1.33:3.67:0.48. IR (ATR): $\tilde{\nu}$ = 3095 (w), 1576 (m), 1462 (s), 1348 (s), 1171 (s), 1131 (m), 921 (m), 853 (w), 817 (w), 533 (m), 425 (w), 326 (w), 301 (m), 224 cm^{-1} (s); UV/Vis-NIR: λ_{max} = 371, 575, 745, 975, 1460 nm; BET surface area (Ar, 87.3 K): 3066 $m^2 g^{-1}$.

Co-MFU-4*l*-nitrate (6-NO_3): Purple powder. Zn/Co/Cl ratio: 1.12:3.88:0.19. IR (ATR): $\tilde{\nu}$ = 1568 (m), 1461 (s), 1348 (s), 1240 (w), 1171 (s), 989 (w), 921 (m), 852 (w), 805 (w), 533 (m), 428 (w), 352 (w), 301 (m), 278 (m), 246 (m), 226 cm^{-1} (s); UV/Vis-NIR: λ_{max} = 366, 566, 721, 954, 1441 nm; BET surface area (Ar, 87.3 K): 3049 $m^2 g^{-1}$.

Co-MFU-4*l*-triflate (6-OTf): Purple powder. Zn/Co/Cl ratio: 1.19:3.81:0.51. IR (ATR): $\tilde{\nu}$ = 1577 (m), 1461 (s), 1348 (s), 1235 (m), 1174 (s), 1028 (m), 921 (m), 854 (w), 805 (w), 764 (w), 639 (m), 576 (w), 532 (m), 429 (w), 353 (w), 302 (m), 280 (m), 228 cm^{-1} (s); UV/Vis-NIR: λ_{max} = 354, 574, 754, 1391 nm; BET surface area (Ar, 87.3 K): 2603 $m^2 g^{-1}$.

Co-MFU-4*l*-formate (6-HCOO): Purple powder. Zn/Co/Cl ratio: 0.88:4.12:0.05; IR (ATR): $\tilde{\nu}$ = 3098 (w), 1577 (s), 1460 (s), 1348 (s), 1299 (m), 1242 (m), 1171 (s), 921 (m), 851 (w), 803 (w), 532 cm^{-1} (m); UV/Vis-NIR: λ_{max} = 363, 561, 756, 1051, 1448 nm; BET surface area (Ar, 87.3 K): 2805 $m^2 g^{-1}$.

Co-MFU-4*l*-azide (6-N_3): Blue powder. Zn/Co/Cl ratio: 1.01:3.99:0.23. IR (ATR): $\tilde{\nu}$ = 3078 (w), 2068 (s), 1575 (m), 1461 (s), 1349 (s), 1219 (w), 1199 (m), 1169 (s), 919 (m), 862 (w), 818 (w), 533 (m), 442 (m), 353 (w), 304 (m), 280 (m), 246 (m), 226 cm^{-1} (s); UV/Vis-NIR: λ_{max} = 389, 563, 612, 659, 854, 1347 nm; BET surface area (Ar, 77.3 K): 2252 $m^2 g^{-1}$.

Co-MFU-4*l*-acetate (6-OAc): Purple powder. Zn/Co/Cl ratio: 0.89:4.11:0.04. IR (ATR): $\tilde{\nu}$ = 3095 (w), 1575 (s), 1460 (s), 1347 (s), 1240 (w), 1173 (s), 920 (m), 851 (w), 815 (w), 688 (m), 619 (w), 532 cm^{-1} (m); BET surface area (N_2, 77.3 K): 2601 $m^2 g^{-1}$.

Co-MFU-4*l*-isocyanate (6-NCO): Blue powder. Zn/Co/Cl ratio: 0.96:4.04:2.28. IR (ATR): $\tilde{\nu}$ = 3095 (w), 2217 (m), 1576 (s), 1460 (s), 1347 (s), 1170 (s), 919 (m), 855 (w), 805 (w), 532 (m), 427 (m), 384 (w), 303 (m), 225 cm^{-1} (s); UV/Vis-NIR: λ_{max} = 602, 856, 1383 nm; BET surface area (N_2, 77.3 K): 1649 $m^2 g^{-1}$.

Mn_2-MFU-4*l*-formate (1-HCOO): Pale-yellow powder. Zn/Mn/Cl ratio: 2.78:2.22:0.74. IR (ATR): $\tilde{\nu}$ = 3093 (w), 1577 (s), 1461 (s), 1348 (s), 1216 (m), 1195 (m), 1168 (s), 921 (m), 854 (m), 807 (w), 531 (m), 427 cm^{-1} (w); BET surface area (N_2, 77.3 K): 3352 $m^2 g^{-1}$.

Fe_2-MFU-4*l*-formate (2-HCOO): Yellow powder. Zn/Fe/Cl ratio: 3.54:1.46:0.87. IR (ATR): $\tilde{\nu}$ = 3095 (w), 1577 (s), 1461 (s), 1349 (s), 1200 (m), 1173 (s), 921 (m), 854 (w), 805 (w), 532 (m), 426 cm^{-1} (w); UV/Vis-NIR: λ_{max} = 968, 1728 nm; BET surface area (N_2, 77.3 K): 3306 $m^2 g^{-1}$.

Ni_2-MFU-4*l*-formate (4-HCOO): Green powder. Zn/Ni/Cl ratio: 2.84:2.16:0.72. IR (ATR): $\tilde{\nu}$ = 3099 (w), 1577 (s), 1461 (s), 1351 (s), 1303 (w), 1244 (w), 1182 (s), 922 (m), 865 (w), 816 (w), 535 cm^{-1} (m); UV/Vis-NIR: λ_{max} = 417, 523, 997 nm; BET surface area (N_2, 77.3 K): 3246 $m^2 g^{-1}$.

Mn_2-MFU-4*l*-fluoride (1-F): Pale-yellow powder. Zn/Mn/Cl ratio: 3.20:1.80:1.26. IR (ATR): $\tilde{\nu}$ = 3078 (w), 1577 (w), 1460 (s), 1349 (s), 1171 (s), 919 (m), 868 (w), 815 (w), 578 (w), 530 (m), 478 (w), 428 cm^{-1} (w); BET surface area (N_2, 77.3 K): 3148 $m^2 g^{-1}$.

Fe_2-MFU-4*l*-fluoride (2-F): Orange-grey powder. Zn/Fe/Cl ratio: 3.59:1.41:2.46. IR (ATR): $\tilde{\nu}$ = 3079 (w), 1577 (w), 1460 (s), 1350 (s), 1239 (m), 1204 (m), 1177 (s), 920 (m), 868 (m), 817 (w), 532 (m), 429 cm^{-1} (w); UV/Vis-NIR: λ_{max} = 372 nm; BET surface area (Ar, 87.3 K): 3505 $m^2 g^{-1}$.

Ni_2-MFU-4*l*-fluoride (4-F): Pale-red powder, turns quickly to pale green in air. Zn/Ni/Cl ratio: 2.86:2.14:1.93. IR (ATR): $\tilde{\nu}$ = 3079 (w), 1576 (w), 1461 (s), 1351 (s), 1240 (w), 1183 (s), 1061 (w), 920 (m), 868 (w), 808 (w), 534 cm^{-1} (m); UV/Vis-NIR: λ_{max} = 697, 868 nm; BET surface area (N_2, 77.3 K): 2977 $m^2 g^{-1}$.

Cu_2-MFU-4*l*-fluoride (5-F): Green-grey powder. Zn/Cu/Cl ratio: 2.84:2.16:1.72. IR (ATR): $\tilde{\nu}$ = 3080 (w), 1576 (w), 1460 (s), 1349 (s), 1179 (s), 919 (s), 868 (m), 808 (m), 533 (m), 428 cm^{-1} (w); UV/Vis-NIR: λ_{max} = 353, 763, 1054 nm; BET surface area (N_2, 77.3 K): 3480 $m^2 g^{-1}$.

Co-MFU-4*l*-fluoride (6-F): Blue-violet powder. Zn/Co/Cl ratio: 1.04:3.96:0.34. IR (ATR): $\tilde{\nu}$ = 3078 (w), 1576 (w), 1460 (s), 1348 (s), 1171 (s), 917 (s), 867 (m), 805 (w), 594 (m), 532 (m), 429 cm^{-1} (w); UV/Vis-NIR: λ_{max} = 359, 547, 645, 834, 1361 nm; BET surface area (N_2, 77.3 K): 2524 $m^2 g^{-1}$.

General procedure for the catalytic oxidation of ethylbenzene: MFU-4*l* derivative (0.1 mmol, based on Mn, Fe, Co, Ni or Cu centers) was added to a solution of ethylbenzene (1.06 g, 10 mmol), *N*-hydroxyphthalimide (163 mg, 1 mmol) and 1,2,4-trichlorobenzene (907 mg, 5 mmol, used as a standard) in acetonitrile/water (98:2) mixture (30 mL) and the mixture was stirred at 40 °C. The conversion was followed by GC/MS. For analysis, 0.1 mL of mixture was filtered through a short pad of neutral Al_2O_3, which was then eluted with Et_2O/CH_2Cl_2/MeOH (10:10:1) mixture. Each analysis was repeated three times. In the case of **5** and **6**, the catalyst was filtered off after the reaction, washed with acetonitrile, DMF, methanol, and CH_2Cl_2, and dried in vacuum. EDX analysis of **5**: Zn/Cu/Cl ratio: 2.81:2.19:2.78. EDX analysis of **6**: Zn/Co/Cl ratio: 0.99:4.01:1.95.

Thermal transformations of MFU-4*l*-formates under N_2: MFU-4*l*-formates (approx. 10 mg) were heated under N_2 gas flow (90 mL min^{-1}) up to 300–350 °C with a heating rate 5 K min^{-1} using a TA Instruments Q500 analyzer and kept at this temperature for 15 min.

Thermal transformations of 6-HCOO and 6-N_3 under CO: Framework **6-HCOO** or **6-N_3** (approx. 5 mg) was heated under CO/Ar (1/9) gas flow (50 mL min^{-1}) up to 325 or 300 °C, respectively, with a heating rate 5 K min^{-1} using a Netzsch STA 409 simultaneous thermal analyzer and kept at this temperature for 15 min.

Preparation of Cu^I-MFU-4*l* through the solvothermal reduction of 5 in DMF: Framework **5** (150 mg) was heated in DMF (25 mL) for 10 h at 140 °C in a sealed tube (until the green color of a solid has disappeared completely). The yellow precipitate was filtered off, washed with DMF, methanol, and dichloromethane and dried at 150 °C under vacuum. Yield 140 mg. Zn/Cu/Cl ratio: 2.43:2.57:2.17. IR (ATR): $\tilde{\nu}$ = 3079 (w), 1577 (w), 1462 (s), 1351 (s),

1204 (m), 1176 (s), 918 (m), 869 (w), 838 (w), 817 (w), 534 (m), 427 cm^{-1} (w); BET surface area (Ar, 87.3 K): 2615 $m^2 g^{-1}$.

Preparation of Cu^I-MFU-4*l* from MFU-4*l* through metal exchange: Copper (I) chloride (149 mg, 1.5 mmol) and lithium chloride (191 mg, 4.5 mmol)) were stirred under nitrogen in *N*,*N*-dimethylacetamide (30 mL) for 1 h at RT. Undissolved CuCl was filtered off through a syringe filter and MFU-4*l* (100 mg, 0.08 mmol) was added to the solution. The reaction mixture was heated for 20 h at 60 °C in a sealed tube. The pale-brown precipitate was filtered off, washed with *N*,*N*-dimethylacetamide, methanol and dichloromethane and dried at 150 °C under vacuum. Zn/Cu/Cl ratio: 3.96:1.04:3.08. IR (ATR): $\tilde{\nu}$ = 3080 (w), 1576 (w), 1461 (s), 1350 (s), 1174 (s), 917 (m), 867 (w), 813 (w), 534 (m), 427 cm^{-1} (w); BET surface area (Ar, 87.3 K): 3944 $m^2 g^{-1}$.

Preparation of Cu^I-MFU-4*l* through the heterogeneous reaction of 5-F with H_2: Framework **5-F** (approx. 10 mg) was heated under H_2/Ar (1:9) gas flow (90 mL min^{-1}) up to 240 °C with a heating rate 5 K min^{-1} using a TA Instruments Q500 analyzer and kept at this temperature for 15 min. A dark-grey powder was obtained. IR (ATR): $\tilde{\nu}$ = 3081 (w), 1577 (w), 1461 (s), 1350 (s), 1175 (s), 1051 (w), 918 (m), 868 (w), 816 (w), 534 (m), 426 cm^{-1} (w); BET surface area (Ar, 87.3 K): 3682 $m^2 g^{-1}$; elemental analysis calcd (%) for $C_{36}H_{12}Cl_2N_{18}O_{10}Cu_2Zn_3$ (Cu^I-MFU-4*l*·2 O_2): C 34.57, H 0.97, N 20.16; found: C 34.68, H 1.19, N 20.35.

Heterogeneous reaction of 5 with H_2: Framework **5** (approx. 10 mg) was heated under H_2/Ar (1:9) gas flow (90 mL min^{-1}) up to 350 °C with a heating rate 5 K min^{-1} using a TA Instruments Q500 analyzer and kept at this temperature for 15 min. A dark-grey powder was obtained. BET surface area (Ar, 87.3 K): 2078 $m^2 g^{-1}$; elemental analysis calcd (%) for $C_{36}H_{12}Cl_2N_{18}O_{10}Cu_2Zn_3$ (Cu^I-MFU-4*l*·2 O_2): C 34.57, H 0.97, N 20.16; found: C 35.26; H 1.20; N 18.95.

Thermal decomposition of 5 under N_2: Framework **5** (approx. 10 mg) was heated under N_2 gas flow (90 mL min^{-1}) up to 400 °C with a heating rate 5 K min^{-1} using a TA Instruments Q500 analyzer and kept at this temperature for 15 min. A dark-grey powder was obtained. BET surface area (Ar, 87.3 K): 2054 $m^2 g^{-1}$; elemental analysis calcd (%) for $C_{36}H_{12}Cl_2N_{18}O_{10}Cu_2Zn_3$ (Cu^I-MFU-4*l*·2 O_2): C 34.57, H 0.97, N 20.16; found: C 35.05, H 1.13, N 18.30.

Acknowledgements

We gratefully acknowledge funding by the priority program 1362 "Porous Metal-Organic Frameworks (MOFs)" of the Deutsche Forschungsgemeinschaft (DFG).

Keywords: heterogeneous catalysis · hydrogen · ligands · metal–organic frameworks · transition metals

[1] H. Furukawa, K. E. Cordova, M. O'Keeffe, O. M. Yaghi, *Science* **2013**, *341*, 1230444.

[2] a) K. Sumida, D. L. Rogow, J. A. Mason, T. M. McDonald, E. D. Bloch, Z. R. Herm, T.-H. Bae, J. R. Long, *Chem. Rev.* **2012**, *112*, 724–781; b) E. Barea, C. Montoro, J. A. R. Navarro, *Chem. Soc. Rev.* **2014**, *43*, 5419–5430.

[3] a) J.-R. Li, J. Sculley, H.-C. Zhou, *Chem. Rev.* **2012**, *112*, 869–932; b) M. P. Suh, H. J. Park, T. K. Prasad, D.-W. Lim, *Chem. Rev.* **2012**, *112*, 782–835; c) Y. Peng, V. Krungleviciute, I. Eryazici, J. T. Hupp, O. K. Farha, T. Yildirim, *J. Am. Chem. Soc.* **2013**, *135*, 11887–11894.

[4] a) J. Gascon, A. Korma, F. Kapteijn, F. X. L. i. Xamena, *ACS Catal.* **2014**, *4*, 361–378; b) J. Liu, L. Chen, H. Cui, J. Zhang, L. Zhang, C.-Y. Su, *Chem. Soc. Rev.* **2014**, *43*, 6011–6061; c) Z.-Y. Gu, J. Park, A. Raiff, Z. Wei, H.-C. Zhou, *ChemCatChem* **2014**, *6*, 67–75; d) K. Leus, Y.-Y. Liu, P. Van Der Voort, *Catal. Rev.* **2014**, *56*, 1–56; e) P. García-García, M. Müller, A. Corma, *Chem. Sci.* **2014**, *5*, 2979–3007.

[5] L. E. Kreno, K. Leong, O. K. Farha, M. Allendorf, R. P. Van Duyne, J. T. Hupp, *Chem. Rev.* **2012**, *112*, 1105–1125.

[6] Y. Cui, Y. Yue, G. Qian, B. Chen, *Chem. Rev.* **2012**, *112*, 1126–1162.

[7] W. Zhang, R.-G. Xiong, *Chem. Rev.* **2012**, *112*, 1163–1195.

[8] C. Wang, T. Zhang, W. Lin, *Chem. Rev.* **2012**, *112*, 1084–1104.

[9] P. Horcajada, R. Gref, T. Baati, P. K. Allan, G. Maurin, P. Couvreur, G. Férey, R. E. Morris, C. Serre, *Chem. Rev.* **2012**, *112*, 1232–1268.

[10] S. M. Cohen, *Chem. Rev.* **2012**, *112*, 970–1000.

[11] J. D. Evans, C. J. Sumby, C. J. Doonan, *Chem. Soc. Rev.* **2014**, *43*, 5933–5951.

[12] a) Y. Han, J.-R. Li, Y. Xie, G. Guo, *Chem. Soc. Rev.* **2014**, *43*, 5952–5981; b) P. Deria, J. E. Mondloch, O. Karagiaridi, W. Bury, J. T. Hupp, O. K. Farha, *Chem. Soc. Rev.* **2014**, *43*, 5896–5912.

[13] C. K. Brozek, M. Dincâ, *Chem. Soc. Rev.* **2014**, *43*, 5456–5467.

[14] D. Denysenko, T. Werner, M. Grzywa, A. Puls, V. Hagen, G. Eickerling, J. Jelic, K. Reuter, D. Volkmer, *Chem. Commun.* **2012**, *48*, 1236–1238.

[15] D. Denysenko, M. Grzywa, J. Jelic, K. Reuter, D. Volkmer, *Angew. Chem. Int. Ed.* **2014**, *53*, 5832–5836.

[16] D. Denysenko, M. Grzywa, M. Tonigold, B. Streppel, I. Krkljus, M. Hirscher, E. Mugnaioli, U. Kolb, J. Hanss, D. Volkmer, *Chem. Eur. J.* **2011**, *17*, 1837–1848.

[17] C. K. Brozek, L. Bellarosa, T. Soejima, T. V. Klark, N. López, M. Dincâ, *Chem. Eur. J.* **2014**, *20*, 6871–6874.

[18] S. Biswas, M. Grzywa, H. P. Nayek, S. Dehnen, I. Senkovska, S. Kaskel, D. Volkmer, *Dalton Trans.* **2009**, 6487–6495.

[19] P. Schmieder, D. Denysenko, M. Grzywa, B. Baumgärtner, I. Senkovska, S. Kaskel, G. Sastre, L. van Wüllen, D. Volkmer, *Dalton Trans.* **2013**, *42*, 10786–10797.

[20] a) S. Biswas, M. Tonigold, D. Volkmer, *Z. Anorg. Allg. Chem.* **2008**, *634*, 2532–2538; b) S. Biswas, M. Tonigold, M. Speldrich, P. Kögerler, M. Weil, D. Volkmer, *Inorg. Chem.* **2010**, *49*, 7424–7434; c) Y.-Y. Liu, M. Grzywa, M. Tonigold, G. Sastre, T. Schüttrigkeit, N. S. Leeson, D. Volkmer, *Dalton Trans.* **2011**, *40*, 5926–5938.

[21] S. Trofimenko, *Chem. Rev.* **1993**, *93*, 943–980.

[22] a) A. Soleimani Dorcheh, D. Denysenko, D. Volkmer, W. Donner, M. Hirscher, *Microporous Mesoporous Mater.* **2012**, *162*, 64–68; b) A. Soleimani-Dorcheh, R. E. Dinnebier, A. Kuc, O. Magdysyuk, F. Adams, D. Denysenko, T. Heine, D. Volkmer, W. Donner, M. Hirscher, *Phys. Chem. Chem. Phys.* **2012**, *14*, 12892–12897; c) O. V. Magdysyuk, D. Denysenko, I. Weinrauch, D. Volkmer, M. Hirscher, R. E. Dinnebier, *Chem. Commun.* **2014**, *51*, 714–717.

[23] J. Teufel, H. Oh, M. Hirscher, M. Wahiduzzaman, L. Zhechkov, A. Kuc, T. Heine, D. Denysenko, D. Volkmer, *Adv. Mater.* **2013**, *25*, 635–639.

[24] A. B. P. Lever, in *Inorganic Electronic Spectroscopy*, 2nd ed., Elsevier, Amsterdam, **1984**.

[25] J. V. Quagliano, A. K. Banerjee, V. L. Goedken, L. M. Vallarino, *J. Am. Chem. Soc.* **1970**, *92*, 482–488.

[26] P. J. Desrochers, J. Telser, S. A. Zvyagin, A. Ozarowski, J. Krzystek, D. A. Vicic, *Inorg. Chem.* **2006**, *45*, 8930–8941.

[27] K. Fujisawa, H. Iwamoto, K. Tobita, Y. Miyashita, K.-i. Okamoto, *Inorg. Chim. Acta* **2009**, *362*, 4500–4509.

[28] S. Hikichi, Y. Sasakura, M. Yoshizawa, Y. Ohzu, Y. Moro-oka, M. Akita, *Bull. Chem. Soc. Jpn.* **2002**, *75*, 1255–1262.

[29] W. G. Jackson, A. M. Sargeson, in *Rearrangements in Ground and Excited States* (Ed.: P. de Mayo), Vol. 2, Academic Press, New York, **1980**, pp. 273–378.

[30] I. R. Beattie, D. P. N. Satchell, *Trans. Faraday Soc.* **1956**, *52*, 1590–1593.

[31] S. Thyagarajan, C. D. Incarvito, A. L. Rheingold, K. H. Theopold, *Inorg. Chim. Acta* **2003**, *345*, 333–339.

[32] D. J. Harding, P. Harding, R. Daengngern, S. Yimklan, H. Adams, *Dalton Trans.* **2009**, 1314–1320.

[33] J. A. Dunne, R. Mariwala, M. Rao, S. Sircar, R. J. Gorte, A. L. Myers, *Langmuir* **1996**, *12*, 5888–5895.

[34] J. Jelic, D. Denysenko, D. Volkmer, K. Reuter, *New J. Phys.* **2013**, *15*, 115004 .

[35] I. Hermans, L. Vereecken, P. A. Jacobs, J. Peeters, *Chem. Commun.* **2004**, 1140–1141.

[36] Y. Ishii, S. Sakaguchi, T. Iwahama, *Adv. Synth. Catal.* **2001**, *343*, 393–427.

[37] M. Tonigold, Y. Lu, A. Mavrandonakis, A. Puls, R. Staudt, J. Möllmer, J. Sauer, D. Volkmer, *Chem. Eur. J.* **2011**, *17*, 8671 – 8695.
[38] A. Dhakshinamoorthy, M. Alvaro, H. Garcia, *Chem. Eur. J.* **2011**, *17*, 6256 – 6262.
[39] S. Biswas, M. Maes, A. Dhakshinamoorthy, M. Feyand, D. E. De Vos, H. Garcia, N. Stock, *J. Mater. Chem.* **2012**, *22*, 10200 – 10209.
[40] O. M. Reinaud, K. H. Theopold, *J. Am. Chem. Soc.* **1994**, *116*, 6979 – 6980.
[41] R. A. Eikey, M. M. Abu-Omar, *Coord. Chem. Rev.* **2003**, *243*, 83 – 124.
[42] a) B. Hinnemann, J. K. Nørskov, *Top. Catal.* **2006**, *37*, 55 – 70; b) L. C. Seefeldt, B. M. Hoffman, D. R. Dean, *Annu. Rev. Biochem.* **2009**, *78*, 701 – 722.
[43] J. du Bois, C. S. Tomooka, J. Hong, E. M. Carreira, *Acc. Chem. Res.* **1997**, *30*, 364 – 372.
[44] C. C. Hojilla Atienza, A. C. Bowman, E. Lobkovsky, P. J. Chirik, *J. Am. Chem. Soc.* **2010**, *132*, 16343 – 16345.
[45] a) Y.-J. Kim, Y.-S. Kwak, S.-W. Lee, *J. Organomet. Chem.* **2000**, *603*, 152 – 160; b) D. Sellmann, F. Geipel, F. W. Heinemann, *Chem. Eur. J.* **2000**, *6*, 4279 – 4284.
[46] G. V. Goeden, K. G. Kaulton, *J. Am. Chem. Soc.* **1981**, *103*, 7354 – 7355.
[47] W. S. Mahoney, D. M. Brestensky, J. M. Stryker, *J. Am. Chem. Soc.* **1988**, *110*, 291 – 293.
[48] T. Liu, X. Wang, C. Hoffmann, D. L. DuBois, R. M. Bullock, *Angew. Chem. Int. Ed.* **2014**, *53*, 5300 – 5304; *Angew. Chem.* **2014**, *126*, 5404 – 5408.
[49] a) M. B. Mooiman, J. M. Pratt, *J. Chem. Soc. Chem. Commun.* **1981**, 33 – 34; b) E. B. Hulley, K. D. Welch, A. M. Appel, D. L. DuBois, R. M. Bullock, *J. Am. Chem. Soc.* **2013**, *135*, 11736 – 11739; c) R. A. Kinney, D. G. H. Hetterscheid, B. S. Hanna, R. R. Schrock, B. M. Hoffman, *Inorg. Chem.* **2010**, *49*, 704 – 713; d) G. J. Kubas, *Adv. Inorg. Chem.* **2004**, *56*, 127 – 177; e) K. Q. A. Leñero, Y. Guari, P. C. J. Kamer, P. W. N. M. van Leeuwen, B. Donnadieu, S. Sabo-Etienne, B. Chaudret, M. Lutz, A. L. Spek, *Dalton Trans.* **2013**, *42*, 6495 – 6512.
[50] a) V. Blum, R. Gehrke, F. Hanke, P. Havu, V. Havu, X, Ren, K. Reuter, M. Scheffler, *Comput. Phys. Commun.* **2009**, *180*, 2175 – 2196; b) X. Ren, P. Rinke, V. Blum, J. Wieferink, A. Tkatchenko, A. Sanfilippo, K. Reuter, M. Scheffler, *New J. Phys.* **2012**, *14*, 053020.
[51] J. P. Perdew, K. Burke, M. Ernzerhof, *Phys. Rev. Lett.* **1996**, *77*, 3865 – 3868.
[52] a) A. D. Becke, *J. Chem. Phys.* **1993**, *98*, 5648 – 5652; b) P. J. Stephens, J. F. Devlin, C. F. Chabalowski, M. J. Frisch, *J. Chem. Phys.* **1994**, *98*, 11623 – 11627.
[53] A. Tkatchenko, M. Scheffler, *Phys. Rev. Lett.* **2009**, *102*, 073005.